Journal of Magnetic Resonance 206 (2010) 210–218

Contents lists available at ScienceDirect

Journal of Magnetic Resonance

journal homepage: www.elsevier.com/locate/jmr

In vivo ^{13}C spectroscopy in the rat brain using hyperpolarized [1-^{13}C]pyruvate and [2-^{13}C]pyruvate

Małgorzata Marjańska *, Isabelle Iltis, Alexander A. Shestov, Dinesh K. Deelchand, Christopher Nelson, Kâmil Uğurbil, Pierre-Gilles Henry

Center for Magnetic Resonance Research and Department of Radiology, University of Minnesota, 2021 6th ST SE, Minneapolis, MN 55455, United States

ARTICLE INFO

Article history:
Received 18 February 2010
Revised 10 July 2010
Available online 16 July 2010

Keywords:
DNP
Time courses
Pyruvate
Lactate
Bicarbonate

ABSTRACT

The low sensitivity of ^{13}C spectroscopy can be enhanced using dynamic nuclear polarization. Detection of hyperpolarized [1-^{13}C]pyruvate and its metabolic products has been reported in kidney, liver, and muscle. In this work, the feasibility of measuring ^{13}C signals of hyperpolarized ^{13}C metabolic products in the rat brain *in vivo* following the injection of hyperpolarized [1-^{13}C]pyruvate and [2-^{13}C]pyruvate is investigated. Injection of [2-^{13}C]pyruvate led to the detection of [2-^{13}C]lactate, but no other downstream metabolites such as TCA cycle intermediates were detected. Injection of [1-^{13}C]pyruvate enabled the detection of both [1-^{13}C]lactate and [^{13}C]bicarbonate. A metabolic model was used to fit the hyperpolarized ^{13}C time courses obtained during infusion of [1-^{13}C]pyruvate and to determine the values of V_{PDH} and V_{LDH}.

1. Introduction

Carbon-13 spectroscopy combined with the infusion of ^{13}C-labeled substrates is a powerful tool to study brain metabolism *in vivo*. Measurement of the incorporation of ^{13}C label from substrates ([1-^{13}C]glucose or [2-^{13}C]acetate for example) into brain metabolites (glutamate, glutamine) has allowed the determination of a variety of metabolic fluxes, such as the rate of neuronal and glial tricarboxylic acid (TCA) cycle, the rate of pyruvate carboxylase, and the rate of glutamate–glutamine cycling between neurons and astrocytes (see [1] and references therein). In spite of these remarkable achievements, ^{13}C magnetic resonance spectroscopy (MRS) remains limited by its low sensitivity. As a result, most *in vivo* ^{13}C experiments require long acquisition times during prolonged infusion of highly-enriched ^{13}C-labeled substrates.

One way of increasing the sensitivity of MR is to create a non-Boltzmann spin state population or hyperpolarization. Hyperpolarization has been accomplished using several methods: brute-force polarization by subjecting a sample to a very strong magnetic field at a temperature close to absolute zero [2], optical pumping [3,4], para-hydrogen induced polarization (PHIP, also called PASADENA) [5–8], and dynamic nuclear polarization (DNP) [9,10]. The optical pumping method is practically limited to noble gas isotopes with spin-1/2 nuclei. The PHIP method can produce more than 20% polarization in a few seconds but is limited to molecules which contain either double or triple carbon–carbon bonds. In contrast, the DNP method, during which a solid-state sample is placed in liquid helium, requires 30–60 min to reach the same degree of polarization as PHIP method; however, DNP can be applied to all nuclei (^{13}C, ^{15}N, etc.) in many molecules. It has been shown recently that the DNP method can enhance the signal-to-noise by a factor over a 10,000 times compared to a conventional NMR experiment in the solution-state [11,12].

The *in vivo* hyperpolarized ^{13}C studies performed to date can be divided into two groups. In the first group, the injection of hyperpolarized substances, which remain in blood vessels and are not quickly metabolized, has been used to obtain very high resolution images of vasculature and perfusion. This type of experiments have been reported using PHIP hyperpolarized substrates in rats [7,13], rabbits [14,15], guinea pigs [16], and pigs [17–19], and using DNP hyperpolarized substrates in rats [12,20–23] and pigs [24]. In the second class of experiments, substances which are quickly metabolized have been used to obtain metabolic information by detecting the formation of hyperpolarized metabolic products. Such experiments have been reported *in vivo* after injection of hyperpolarized [1-^{13}C]pyruvate in rats [25–30], mice [31–33], pigs [25,34] and in isolated rat hearts [35,36], [2-^{13}C]pyruvate in isolated rat hearts [37], [1-^{13}C]lactate in rats [38], ^{13}C-labeled bicarbonate in mice [39], [1-^{13}C]acetate in mice [40], and [5-^{13}C]glutamine in cultured hepatoma cells [41].

* Corresponding author. Fax: +1 612 626 2004.
E-mail addresses: gosia@cmrr.umn.edu (M. Marjańska), isabelle@cmrr.umn.edu (I. Iltis), shestov@cmrr.umn.edu (A.A. Shestov), dinesh@cmrr.umn.edu (D.K. Deelchand), nelsonc25@gmail.com (C. Nelson), kamil@cmrr.umn.edu (K. Uğurbil), henry@cmrr.umn.edu (P.-G. Henry).

1090-7807/$ - see front matter © 2010 Elsevier Inc. All rights reserved.
doi:10.1016/j.jmr.2010.07.006

In the aforementioned studies, administration of the hyperpolarized [1-^{13}C]pyruvate was shown to result in a sparse spectrum composed of the pyruvate substrate and its products, [1-^{13}C]lactate (via lactate dehydrogenase (LDH)), [1-^{13}C]alanine (via alanine aminotransferase), and ^{13}C bicarbonate (via pyruvate dehydrogenase complex (PDH) and carbonic anhydrase) [25]. Additionally, [1-^{13}C]pyruvate hydrate, a metabolically inactive molecule formed during the dissolution process of [1-^{13}C]pyruvate, is present in the spectrum [25]. Increased intratumoral levels of lactate were found following intravenous injection of hyperpolarized [1-^{13}C]pyruvate into rats containing subcutaneously implanted P22 tumors [26]. In contrast to measurements in metabolically active cardiac tissue showing evolution of bicarbonate [34], no bicarbonate was found in those tumors, indicating little PDH activity. Elevated [1-^{13}C]lactate was also observed in both primary and metastatic tumors in a mouse model of prostate cancer [31]. A marked reduction in the lactate to pyruvate ratio and the apparent rate constant of the LDH activity were observed in the drug treated EL-4 tumors implanted in mice [32]. A reduction in PDH activity was reported in the hearts of fasted rats as compared with fed rats suggesting that hyperpolarized ^{13}C spectroscopy is sensitive to physiological perturbations in PDH flux [29]. Up to date, however, attempts to develop metabolic models to fit ^{13}C hyperpolarized data in order to determine metabolic rates remain relatively simple. Metabolic modeling of hyperpolarized pyruvate, lactate, and bicarbonate signals in the brain has not been published so far.

In this study, we investigate metabolism in the rat brain *in vivo* following injection of hyperpolarized [1-^{13}C]pyruvate and [2-^{13}C]pyruvate. We also explore the spatial origin of hyperpolarized ^{13}C signals in the rat brain as well as the influence of decoupling on linewidths and the SNR of [1-^{13}C]pyruvate and [2-^{13}C]pyruvate signals and their metabolic products. In addition, a metabolic model is proposed to fit hyperpolarized lactate and bicarbonate ^{13}C time courses measured after [1-^{13}C]pyruvate injection.

2. Experimental

2.1. Samples

Aliquots (~10 μL) of pure [1-^{13}C]pyruvic acid (Cambridge Isotope Laboratories, Andover, MA) and 15 mM Tris{8-carboxyl-2,2,6,6-tetra(2-(1-hydroxyethyl))-benzo[1,2-d:4,5-d′]bis(dithiole-2-yl)methyl] sodium salt (OX63 trityl radical) and of [2-^{13}C]pyruvic acid (Isotec, Miamisburg, OH) and OX63 trityl radical were placed into liquid helium and hyperpolarized by DNP (HyperSense, Oxford Instruments, UK) in a field strength of 3.35 T at approximately 1.4 K for 90 min (time constant ~700 s) and 120 min (time constant ~1100 s), respectively. [1-^{13}C]pyruvate and [2-^{13}C]pyruvate samples were then dissolved either in (i) 0.32 mM Na_2EDTA solution, (ii) 40 mM TRIS buffer, 40 mM NaOH and 0.32 mM Na_2EDTA solution (buffered solution), or (iii) a buffered solution prepared with D_2O to produce 4 mL of hyperpolarized solutions at a concentration of ~35 mM and a pH of 3 or 7, respectively.

2.2. Phantom

The solution-state polarization and T_1 values at 9.4 T were obtained using an 18-mm outer diameter spherical glass bulb (Wilmad-Labglass, Buena, NJ) into which the hyperpolarized solutions were injected. Injection started about 20 s after dissolution and lasted for 6 s.

Data used to obtain the T_1 values for [1-^{13}C]pyruvate and [2-^{13}C]pyruvate were acquired using a small-flip angle pulse-acquire (4.5° at the coil center, T_R = 3 s, 128 scans) with ^{1}H decoupling.

2.3. Animals

All animal experiments were performed in accordance with the NIH Guide for the Care and Use of Laboratory Animals and were approved by the Institutional Animal Care and Use Committee of the University of Minnesota. Male Sprague–Dawley rats (260–320 g, Charles River Laboratories, Inc.) were placed in an induction chamber ventilated with isoflurane and a 70%:30% N_2O:O_2 mixture. Once unconscious, rats were quickly removed and xylocaine was applied in the throat using a cotton swab, and an 14-gauge catheter was carefully inserted between the vocal cords. The catheter was then connected to the ventilator providing a 70%:30% N_2O:O_2 mixture and 1.8% isoflurane. Body temperature was maintained at 37 °C using a heating pad with warm water circulation. Femoral vein and both arteries were cannulated for infusion of hyperpolarized substances, blood pressure monitoring, and blood sampling, respectively. Femoral vein rather than caudal vein was used for these experiments as previously it was observed that caudal vein catheters tend to clog easily especially when several injections are done in the same animal with extended period of time between each injection. Additionally, femoral vein allowed rapid injection which gave the best chance to observe a high polarization in the brain. Animals were placed in a home-built holder, and the head position was fixed using ear rods and a bite-bar. Blood gases were measured every 20 min to ensure stable physiological conditions.

The animals were injected intravenously with either hyperpolarized [1-^{13}C]pyruvate or [2-^{13}C]pyruvate solutions (~2.2 mL, 34.5 mM). Injection started about 20 s after dissolution and lasted for ~6 s.

2.4. In vivo spectroscopy

All ^{13}C spectra were acquired on a 9.4-T, 31-cm horizontal bore magnet (Magnex Scientific, Oxford, UK) interfaced with a Varian INOVA console (Varian, Palo Alto, CA, USA). The magnet was equipped with a gradient insert capable of reaching 450 mT/m in 200 μs (Resonance Research, Inc., Billerica, MA). The radiofrequency (r.f.) coil assembly consisted of an inner ^{13}C linearly polarized surface coil (12 mm diameter) and a ^{1}H quadrature surface coil (two loops of 14 mm diameter) built according to a previously described design [42]. Gradient echo (T_R = 60 ms; T_E = 3.9 ms; matrix = 256 × 128; slice thickness = 2 mm) images were acquired to select a 9 × 5 × 9 mm^3 volume in the rat brain and a 9 × 1.6 × 16 mm^3 volume including muscle and subcutaneous tissue. For greater anatomical details, T_2-weighted multislice rapid acquisition with relaxation enhancement (RARE) images (T_R = 4 s, T_E = 60 ms, echo train length = 8, matrix 256 × 128, slice thickness = 1 mm, 11 slices) were acquired. Linewidths of water around 18 Hz were obtained in the voxel in the rat brain after adjusting the first- and second-order shims using FAST(EST)MAP [43,44].

The spectra were acquired with one of the following pulse sequences: (1) pulse-acquire with a small or large flip angle (4.5° or 43° at the coil center); (2) 90° BIR4 pulse [45] (6 ms, bandwidth = 3.23 kHz (32.1 ppm) defined as the excitation width where M_{xy} was at least 90% of the desired magnetization, B_{1max} = 2.25 kHz); (3) LASER sequence (localization by adiabatic selective refocusing) [46] adapted for ^{13}C spectroscopy. In LASER, either a 45° or a 90° BIR4 pulse (same as described above) was used for excitation, and six 3 ms hyperbolic secant pulses, HS1, with a bandwidth of 6.67 kHz (66.3 ppm) were used for refocusing. The echo time was 29 ms. ^{1}H decoupling was performed using WALTZ-16 [47] during the acquisition time. All spectra were acquired with 30,000 complex points and spectral width of 50 kHz.

2.5. Modeling

A three-compartment non-steady state brain/blood/body metabolic model (Fig. 1) was used to fit the hyperpolarized ^{13}C time courses of lactate and bicarbonate in order to determine the values of brain V_{PDH}, brain V_{LDH} and the rate of transport of pyruvate through the BBB ($V_{tr\ Pyr\ brain}$).

In the model, the infused hyperpolarized ^{13}C-pyruvate is transported from the blood to the brain and to the body assuming reversible non-steady-state Michaelis–Menten transport kinetics. Within each compartment (brain, blood and body), pyruvate is in exchange with lactate through LDH. Lactate exchanges between compartments following Michaelis–Menten kinetics. Glycolysis, V_{gly}, contributes to the production of unlabeled pyruvate in all three compartments. Pyruvate also produces bicarbonate through V_{PDH} in the brain and in the body (but not in the blood due to the low PDH activity in the blood).

The model was expressed mathematically using two types of dynamic mass balance equations: (1) mass balance for the total concentration of brain, blood, body pyruvate and lactate (six equations), and (2) ^{13}C isotope mass balance for labeled metabolites pyruvate, lactate, and bicarbonate (nine equations). All concentrations and parameters used in the model are listed in the Table 1 along with references. A T_1 relaxation time of 14 s, based on the value obtained for pyruvate from small-flip angle data, was assumed for hyperpolarized pyruvate, lactate and bicarbonate.

The input function for pyruvate and lactate in plasma was calculated based on the concentration and volume of the hyperpolarized solution (34.5 mM and 2.2 mL) injected into the rats (blood volume of ~20 mL in 260–320 g rats) and literature values for V_{LDH} and V_{tr} for lactate and pyruvate in body and brain (Table 1). It was estimated that the concentration (and enrichment) of pyruvate in plasma increased from 0.15 mM to ~3.3 mM (0.011–0.9) in the first 6 s and exponentially decreased to ~0.5 mM (to 0.6) and the concentration of lactate in the plasma increased (apparent hyperbola) from 1 mM (enrichment 0.011) to ~2.5 mM (enrichment 0.6) during the time of experiment.

In vivo time courses of hyperpolarized [1-^{13}C]lactate and ^{13}C-bicarbonate signal intensities were fitted with the metabolic model described above. Based on sensitivity map of the surface coil used in the study and the anatomy of the rat head (superior sagittal sinus close to the surface coil), it was estimated that the blood contributed 10% to the total signal under the experimental conditions of using a 43° flip angle (at the center of the coil).

Three parameters were fitted: $V^{max}_{tr\ Pyr\ brain}$ through BBB, and $V_{PDH\ brain}$ and $V_{LDH\ brain}$ at steady state. Numerical solutions of the ordinary differential equations (ODEs) were obtained using a Runge–Kutta 4th order procedure for stiff systems, and minimizations were done by the Broyden–Fletcher–Goldfarb–Shanno (BFGS) and Simplex algorithms. The errors for the obtained values were estimated using Monte Carlo simulations with experimental noise levels. All numerical procedures were carried out in Matlab.

Table 1
Modeling parameters.

Variable/parameter	Value	References
Concentrations (μmol/g)		
$[Pyr]_{brain}$	0.16	[53]
$[Pyr]_{blood}$	0.1	[54]
$[Pyr]_{body}$	0.15	[55]
$[Lac]_{brain}$	1.2	[56]
$[Lac]_{blood}$	1	[54]
$[Lac]_{body}$	1.1	[57]
$[HCO_3^-]_{brain}$	24	[58]
$[HCO_3^-]_{blood}$	20	[59]
$[HCO_3^-]_{body}$	21	[60]
Fluxes (μmol/g wet weight/min)		
$V_{PDH\ body}$	1.0	Estimated from [61]
$V_{gly\ body}$	0.5	Assumed
$V_{gly\ blood}$	0.03	[62]
$V^{max}_{tr\ Pyr\ body}$	1.0	Estimated from [63,64]
$V^{max}_{tr\ Lac\ body}$	1.5	Estimated from [65,63]
$V^{max}_{tr\ Lac\ brain}$	1.5	Estimated from [65,63]
$V_{tr\ HCO_3^-\ brain}$	3.9	Estimated from [66]
$V_{tr\ HCO_3^-\ body}$	3.9	Estimated from [66]
Michaelis constants (mM)		
$K_{m\ tr\ Pyr\ body/brain}$	0.7	[65]
$K_{m\ tr\ Lac\ body/brain}$	4	[65]
$K_{m\ PDH\ brain\ Pyr}$	0.15	[67]
LDH flux constant (min^{-1})		
Klp_{blood} (related to $V^-_{LDH\ blood}$)	0.19	[62]
$Kpl_{blood}(V^+_{LDH\ blood})$	1.6	[62]
$Klp_{blood}(V^-_{LDH\ blood})$	1.0	[68]
$Kpl_{body}(V^+_{LDH\ blood})$	8	[68]
Relative volumes		
V_{brain}	0.01	Current study
V_{blood}	0.07	[69]
V_{body}(fast component)	0.1	Estimated from [66]

3. Results

3.1. In vitro characterization of hyperpolarized [1-^{13}C]pyruvate and [2-^{13}C]pyruvate solutions

In addition to the peak of [1-^{13}C]pyruvate, [1-^{13}C]pyruvate hydrate and two other resonances were observed at 177.47 ppm and 179.16 ppm. These two resonances, which were also observed

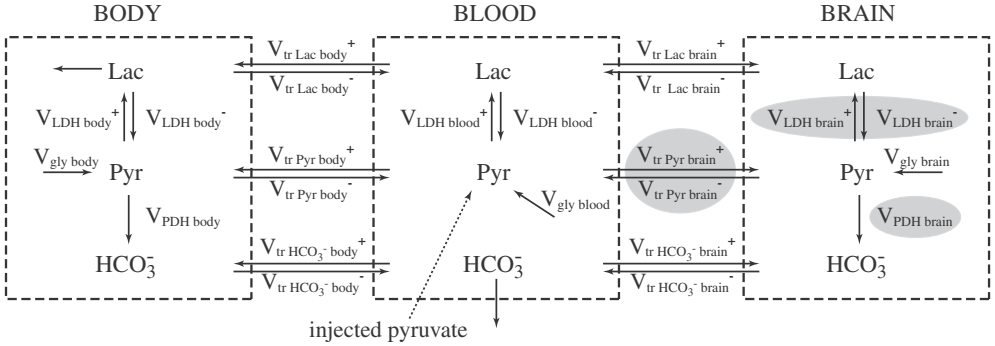

Fig. 1. Three-compartment brain/blood/body metabolic model used to fit the hyperpolarized ^{13}C time courses of lactate and bicarbonate and to determine values of $V_{PDH\ brain}$ and $V_{LDH\ brain}$ and rate of transport of pyruvate through blood–brain-barrier ($V_{tr\ Pyr\ brain}$) (gray balloons). $V_{gly\ body/blood/brain}$ – glycolysis fluxes in body/blood/brain. $V_{tr\ Pyr/Lac/HCO_3^-\ body/brain}{}^+/V_{tr\ Pyr/Lac/HCO_3^-\ body/brain}{}^-$ – transport rates of pyruvate/lactate/bicarbonate to body/brain. $V_{LDH\ body/blood/brain}{}^+/V_{LDH\ body/blood/brain}{}^-$ – lactate dehydrogenase fluxes in body/blood/brain. $V_{PDH\ body/brain}$ – pyruvate dehydrogenase fluxes in body/brain. Pyr – pyruvate, Lac – lactate, HCO_3^- – bicarbonate.

Table 2
Apparent T_1 values for hyperpolarized substances at 9.4 T.

Dissolution solvent	pH	T_1 (s)			
		[1-^{13}C]pyr	[1-^{13}C]pyr hyd	[2-^{13}C]pyr	[2-^{13}C]pyr hyd
H_2O	3	26 ± 9	26 ± 8	21 ± 1	21 ± 1
Buffer with H_2O	7	46 ± 6	37 ± 5	37 ± 1	27 ± 1
Buffer with D_2O	7	57 ± 8	43 ± 2	41 ± 1	34 ± 2

in vivo, were attributed to be impurities. Impurities were also identified in spectra from hyperpolarized [2-^{13}C]pyruvate solutions with peaks observed at 88.19, 143.20 and 172.04 ppm. The polarization levels of [1-^{13}C]pyruvate and [2-^{13}C]pyruvate were measured *in vitro* to be 8% and 5% at a time of measurement, 26 s after dissolution, respectively. The apparent T_1's of [1-^{13}C]pyruvate, [1-^{13}C]pyruvate hydrate, [2-^{13}C]pyruvate, and [2-^{13}C]pyruvate hydrate measured *in vitro* strongly depended upon the pH and on the solvent used for dissolution (Table 2). The T_1 relaxation times were longer at neutral pH than at acidic pH. In addition, the T_1's were longer when D_2O was used to prepare the dissolution buffer instead of H_2O. All *in vivo* experiments were performed with hyperpolarized solutions at neutral pH.

3.2. Effect of decoupling

Most *in vivo* hyperpolarized studies have been utilizing molecules with ^{13}C labeled quaternary carbons. In the most often used [1-^{13}C]pyruvate, ^{13}C labeled carbon does not have any ^{1}H directly attached to it and therefore experiences only a small *J*-coupling with the ^{1}H's three bonds away. In case of [2-^{13}C]pyruvate and [1-^{13}C]lactate, the ^{13}C labeled carbon also does not have any ^{1}H directly attached to it, but it is *J*-coupled to ^{1}H's which are two and three bonds away. The linewidth of [1-^{13}C]pyruvate signal only slightly improved by 1.2 ± 0.3 Hz with broadband ^{1}H decoupling, whereas the linewidth of [1-^{13}C]lactate signal decreased substantially by 6.3 ± 0.6 Hz (Table 3). This is consistent with *J*-coupling constants and the number of protons in each molecule (Table 4). The decrease in linewidth due to ^{1}H decoupling resulted in a corresponding increase in the peak height (or SNR). For *in vivo* linewidth of 6 Hz, the improvement in SNR was 12% for [1-^{13}C]pyruvate, and 76% for [1-^{13}C]lactate. Similarly the linewidth of the [2-^{13}C]pyruvate signal was narrower by 11 ± 2 Hz with decoupling, and the linewidth of each satellite of the [2-^{13}C]lactate signal was narrower by 4 ± 1 Hz (Table 3). The improvement in SNR for [2-^{13}C]pyruvate was 50% and 136% for [2-^{13}C]lactate. The larger improvement for the [2-^{13}C]lactate signal was expected due to the large value of the one-bond *J*-coupling. All *in vivo* experiments were performed with ^{1}H decoupling.

3.3. In vivo brain studies with hyperpolarized [1-^{13}C]pyruvate

After injection of hyperpolarized [1-^{13}C]pyruvate, *in vivo* spectra acquired with a 4.5° pulse angle (at the center of the coil) using the r.f. coil placed over the rat head were dominated by resonances corresponding to [1-^{13}C]pyruvate (172.08 ppm), [1-^{13}C]pyruvate hydrate (180.42 ppm), and [1-^{13}C]lactate (184.3 ppm) (Fig. 2). The infused substances, [1-^{13}C]pyruvate and [1-^{13}C]pyruvate hydrate, peaked 6 s after beginning of the injection. The [1-^{13}C]pyruvate signal then gradually decreased within 60 s, and the [1-^{13}C]pyruvate hydrate signal completely disappeared after 20 s. Formation of hyperpolarized [1-^{13}C]lactate was also observed with a maximum signal around 22 s. The formation of ^{13}C-bicarbonate was detected when a larger pulse flip angle (43° at the coil center) was used (Fig. 3A). The bicarbonate signal also peaked around 22 s after injection, similarly to the lactate signal.

Table 4
Chemical shifts and coupling constants determined from high-resolution ^{13}C NMR spectra.

Molecule	Group	Chemical shift (ppm)	*J*-coupling (Hz)
Pyruvate	^{1}COOH	172.08	$^3J_{C_1-H_3} = 1.32$
	^{2}CO	206.71	$^2J_{C_2-H_3} = 6.2$
	^{3}CH$_3$	29.16	$^1J_{C_3-H_3} = 128.72$
Lactate	^{1}COOH	184.30	$^2J_{C_1-H_2} = 4.06$
			$^3J_{C_1-H_3} = 4.06$
	^{2}CHOH	70.13	$^1J_{C_2-H_2} = 146.30$
			$^2J_{C_2-H_3} = 4.27$
	^{3}CH$_3$	22.17	$^1J_{C_3-H_3} = 127.84$
			$^2J_{C_3-H_2} = 3.56$

The spatial dependence of the observed signals was investigated at a single time point (9 s after beginning of injection) using a LASER sequence with a 90° excitation pulse (Fig. 4A and Fig. 4B). This sequence provided excellent localization and an excellent signal-to-noise ratio. With high signal-to-noise ratio, the [1-^{13}C]alanine signal was observed as a small shoulder to the much stronger signal of an impurity (Fig. 4B). Localized spectra measured in the subcutaneous region showed a strikingly lower lactate to pyruvate ratio (lac:pyr ratio = 14 ± 3%, three animals, four dissolutions) than spectra measured in the brain tissue (lac:pyr ratio = 127 ± 20%, four animals, five dissolutions). The different spectral pattern between the two locations suggests that the detected signals do not arise solely from the blood compartment. If the lactate signal was only coming from the blood, the spectral patterns would be expected to be identical in both voxels. This was also confirmed with preliminary CSI data showing that pyruvate is located primarily in "blood" voxels while lactate is distributed much more uniformly throughout the brain (data not shown).

Consistent with the observation of these regional differences, the lactate to pyruvate ratio in the pulse-acquire spectra was strongly dependent on the angle of the excitation pulse (Fig. 4C and D). Spectra measured using pulse-acquire with a small-flip angle (4.5° at the center of the coil; Fig. 4C) had a very similar lactate to pyruvate ratio (lac:pyr ratio = 21 ± 7%, five animals, 15 dissolutions) to that of the subcutaneous voxel, suggesting that most of the signal comes from the subcutaneous region under these small-flip angle conditions. In contrast, spectra measured with a large excitation flip angle (pulse-acquire with a 90° adiabatic

Table 3
Effect of ^{1}H decoupling on linewidths (reported in Hz) and SNR.

Linewidths[a]						SNR[b]	
Undecoupled		Decoupled		Difference		$S_{decoupled}/S_{undecoupled}$	
[1-^{13}C]pyr	[1-^{13}C]lac	[1-^{13}C]pyr	[1-^{13}C]lac	[1-^{13}C]pyr	[1-^{13}C]lac	[1-^{13}C]pyr	[1-^{13}C]lac
7.2 ± 1.1	12.8 ± 0.9	6.0 ± 1.0	6.4 ± 0.6	1.2 ± 0.3	6.3 ± 0.6	1.12	1.76
[2-^{13}C]pyr	[2-^{13}C]lac	[2-^{13}C]pyr	[2-^{13}C]lac	[2-^{13}C]pyr	[2-^{13}C]lac	[2-^{13}C]pyr	[2-^{13}C]lac
22 ± 4	10 ± 1	11 ± 1	5 ± 1	11 ± 2	4 ± 1	1.50	2.36

[a] Obtained experimentally using LASER sequence.
[b] Obtained using simulations.

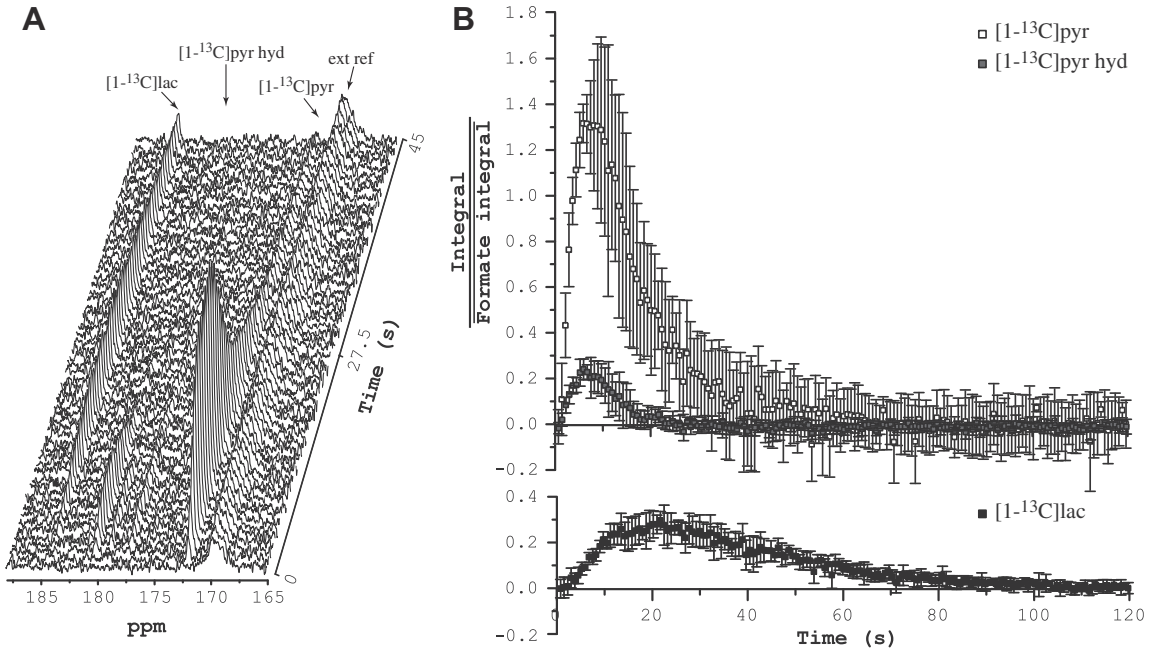

Fig. 2. *In vivo* time courses measured after injection of hyperpolarized [1-^{13}C]pyruvate solution into femoral vein with the r.f. coil placed over the rat head. (A) Representative time course. T_R = 0.75 s, pulse-acquire, 4.5° pulse at the center of the coil, N_{EX} = 60, 7-Hz line-broadening. (B) Average and standard deviation of five time courses of [1-^{13}C]pyruvate, [1-^{13}C]pyruvate hydrate, and [1-^{13}C]lactate (integral of each of the species was scaled by average of external reference's (formic acid) integral). Four animals, pulse-acquire, 4.5° pulse at the center of the coil, T_R = 0.75 s, N_{EX} = 160; ext ref – external reference.

pulse; Fig. 4D) had a much higher lactate to pyruvate ratio (lac:pyr ratio = 46 ± 9%, three animals, four dissolutions), suggesting that a significant fraction of the detected signal came from brain tissue rather than subcutaneous region.

A three-compartment brain/blood/body metabolic model (Fig. 1) was used to fit the time courses of the hyperpolarized [1-^{13}C]lactate and [^{13}C]bicarbonate and to determine the values of brain V_{PDH} and V_{LDH} and the rate of transport of pyruvate through the BBB ($V_{tr\ Pyr\ brain}$) (Fig. 3B and C). $V_{PDH\ brain}$ at steady state was estimated to be 0.9 ± 0.1 μmol/g/min which is in a good agreement with previously reported $V_{PDH\ brain}$ values under similar anesthetic conditions [48]. Apparent $V_{LDH\ brain}$ was estimated to be 1.5 ± 0.4 μmol/g/min which is similar but somewhat lower than 4.8 μmol/g/min reported in the previous study [49]. The value of 4.8 μmol/g/min was derived from the pseudo first-order rate constant (k = 0.08 s^{-1}) reported in that study and using a lactate concentration of 1 mM. $V_{tr\ Pyr\ brain}$ was estimated to be 0.1 μmol/g/min at initial steady-state condition. Additionally, the same three-compartment brain/blood/body metabolic model without pyruvate transport through the BBB ($V^{max}_{tr\ Pyr\ brain} = 0$) was used to fit the time courses of the hyperpolarized [1-^{13}C]lactate and [^{13}C]bicarbonate (Fig. 3B and C). The metabolic model with the transport of pyruvate through the BBB better fitted the [1-^{13}C]lactate time course than the metabolic model without pyruvate transport, but both of the models could potentially explain experimental lactate data. In contrasts, the metabolic model without pyruvate transport through the BBB could not fit the experimental bicarbonate data (with value of $V_{PDH\ brain}$ = 10 μmol/g/min which is an order of magnitude off from physiological range) suggesting that bicarbonate is produced in the brain after transport of pyruvate into the brain. V_{PDH} measured using the bicarbonate signal would therefore reflect brain V_{PDH} activity.

3.4. In vivo brain studies with hyperpolarized [2-^{13}C]pyruvate

[2-^{13}C]pyruvate was successfully hyperpolarized with a buildup time constant around 1100 s (longer than that of [1-^{13}C]pyruvate of ~700 s). After i.v. injection of hyperpolarized [2-^{13}C]pyruvate solution, resonances corresponding to [2-^{13}C]pyruvate (206.71 ppm), [2-^{13}C]pyruvate hydrate (95.57 ppm), and [2-^{13}C]lactate (70.13 ppm) were observed using the r.f. coil placed over the head (Fig. 5A). Infused substances, [2-^{13}C]pyruvate and [2-^{13}C]pyruvate hydrate, peaked 7 s after the beginning of the injection. The [2-^{13}C]pyruvate signal gradually decreased within 40 s, and the [2-^{13}C]pyruvate hydrate signal completely disappeared after 20 s. Formation of hyperpolarized [2-^{13}C]lactate was observed with a highest signal around 12 s and the signal disappeared at 30 s (Fig. 5B). The signal-to-noise ratio of the detected hyperpolarized ^{13}C resonances was lower than that obtained for [1-^{13}C]pyruvate, due to lower solid-state polarization levels obtained for [2-^{13}C]pyruvate as well as the shorter T_1 relaxation times.

Interestingly, an additional peak was detected at 182.8 ppm using the LASER sequence, but only in animals that were fasted overnight (Fig. 6A). This peak was unequivocally and consistently detected in all six fasted rats studied. This signal was not present in the non-fasted rats (Fig. 6B), suggesting that this resonance, probably corresponding to a carboxyl group from fatty acids (likely acetate), might be produced in liver and transported to the brain.

4. Discussion

We report here the ^{13}C hyperpolarized studies in the brain *in vivo*. After injection of a hyperpolarized [1-^{13}C]pyruvate solution in femoral vein, [1-^{13}C]pyruvate, [1-^{13}C]pyruvate hydrate, [1-^{13}C]lactate, [1-^{13}C]alanine, and ^{13}C bicarbonate were detected in the rat brain *in vivo*. After injection of hyperpolarized [2-^{13}C]pyruvate solution, [2-^{13}C]pyruvate, [2-^{13}C]pyruvate hydrate, [2-^{13}C]lactate were also observed in an intact rat brain.

We also successfully hyperpolarized [2-^{13}C]pyruvate, and detected for the first time signals from [2-^{13}C]pyruvate, [2-^{13}C]pyruvate hydrate, and [2-^{13}C]lactate in the brain. Unlike [1-^{13}C]pyruvate in which the labeled carbon is eliminated as $^{13}CO_2$ when converting pyruvate to acetyl-CoA, [2-^{13}C]pyruvate is expected to result in the formation of [1-^{13}C]acetyl-CoA, which

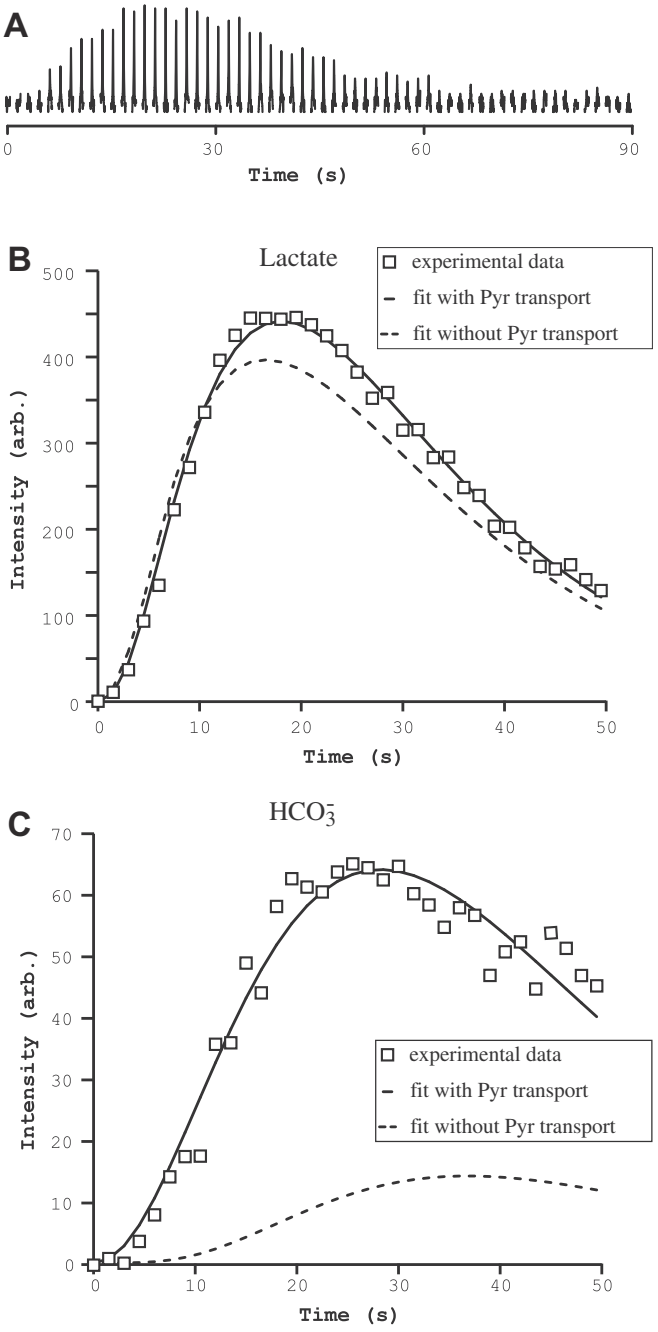

Fig. 3. (A) *In vivo* time course of bicarbonate measured in one representative animal after injection of hyperpolarized [1-^{13}C]pyruvate into femoral vein of the rat. Pulse-acquire, 43° pulse at the center of the coil, 161.5–162.5 ppm, T_R = 1.5 s, N_{EX} = 60, 5-Hz line-broadening. Experimental hyperpolarized ^{13}C time course of lactate (B) and bicarbonate (C) fitted with a three-compartment metabolic model with (continuous line) and without (dashed line) pyruvate transport through the blood–brain-barrier.

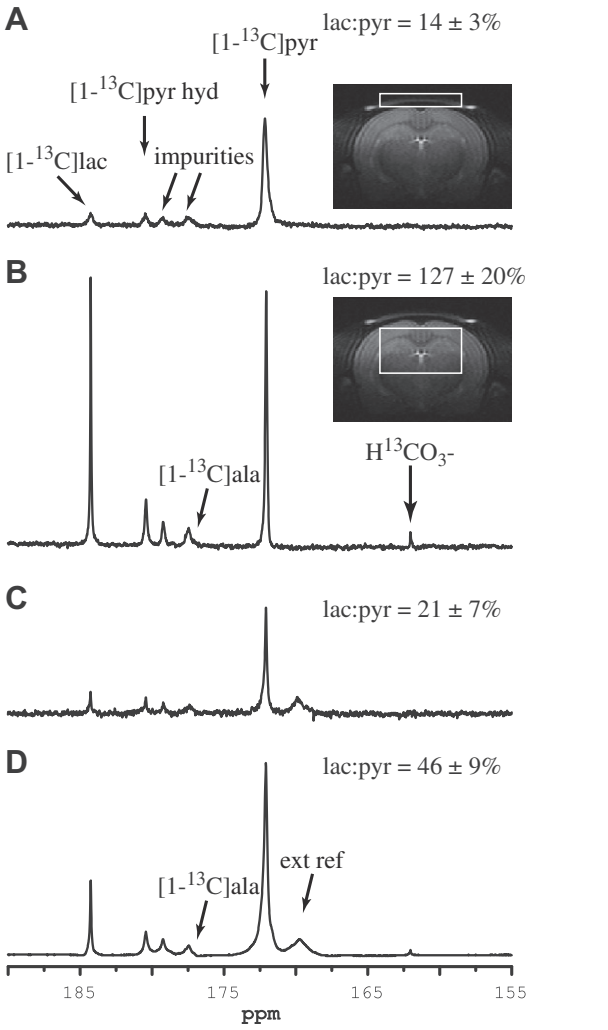

Fig. 4. Spatial origin of hyperpolarized signals. Single-shot *in vivo* ^{1}H decoupled ^{13}C spectra acquired 9 s after beginning of injection of hyperpolarized solution with (A) LASER sequence from 216 μL (9 × 1.6 × 16 mm^3) voxel containing muscle and subcutaneous tissue (insert: RARE image of a rat brain showing the position and size of the localized volume), (B) LASER sequence from 405 μL (9 × 5 × 9 mm^3) voxel containing only brain tissue (insert: RARE image of a rat brain showing the position and size of the localized volume), (C) small-flip angle pulse-acquire (4.5° at the center of the coil), (D) 90° adiabatic BIR4 pulse-acquire. All spectra are shown with 2-Hz line-broadening. The lactate to pyruvate ratio for each spectrum is reported on the right side; ala = alanine.

enters the TCA cycle to form [2-^{13}C]citrate and eventually [5-^{13}C]2-oxoglutarate and [5-^{13}C]glutamate. Using hyperpolarized [1-^{13}C]acetate, small signals (0.1% of the intensity of the injected substance) of acetyl-CoA and acetyl-carnitin have been observed on spectra localized over the heart or liver region in the mice [40]. However, the authors did not observe any other intermediates. Recently, labeling of the TCA cycle intermediates and glutamate was observed in the perfused rat hearts [37]. Several factors could explain the detection of these metabolites in the perfused heart but not in the brain: (1) the brain has slower metabolic rates than the heart, (2) substrates may be delivered more quickly to a perfused organ, (3) the blood–brain barrier slows down delivery of label to the brain, and (4) higher NMR sensitivity of perfused heart experiments compared to *in vivo* brain experiments. Nonetheless, it is possible that future improvements will allow detection of such signals in the brain.

Comparing the localized spectra of subcutaneous tissue with brain voxels revealed very different patterns, especially in the ratio of [1-^{13}C]lactate to [1-^{13}C]pyruvate. The spectrum obtained from the subcutaneous tissue voxel was very similar to the small-flip angle pulse-acquire data. Spectrum obtained from the brain voxel, where [1-^{13}C]lactate signal is higher than the [1-^{13}C]pyruvate signal, was unique, suggesting that the large part comes from brain tissue and not from the blood. The main source of energy for the brain comes from glucose. However, brain can also metabolize other substances under non-physiological conditions such as injection of highly concentrated pyruvate [50], lactate or acetate [51]. The three-compartment body/blood/brain metabolic model suggests that the high amount of lactate detected in the brain tissue

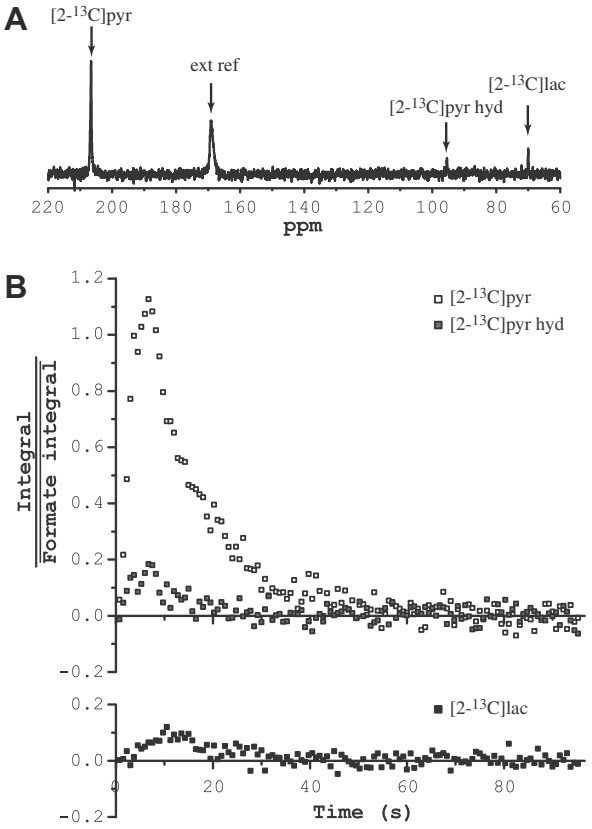

Fig. 5. *In vivo* time courses measured after injection of hyperpolarized [2-^{13}C]pyruvate solution into femoral vein with r.f. coil placed over the rat head. (A) Representative spectrum obtained 12 s after beginning of injections (7-Hz line-broadening). (B) Time course of [2-^{13}C]pyruvate, [2-^{13}C]pyruvate hydrate, and [2-^{13}C]lactate obtained from sum of four dissolutions (integral of each of the species was scaled by average of external reference's (formic acid) integral). Three animals, four dissolutions, pulse-acquire, 4.5° pulse at the center of the coil, T_R = 0.75 s, N_{EX} = 128.

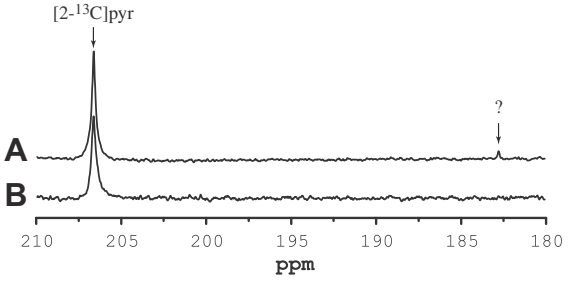

Fig. 6. ^{1}H decoupled localized ^{13}C spectra obtained from a 405 μL (9 × 5 × 9 mm^3) voxel containing brain tissue 18 s after beginning of injection of hyperpolarized [2-^{13}C]pyruvate solution into the femoral vein. Representative spectra acquired from (A) non-fasted and (B) fasted animals. ^{13}C-LASER, T_E = 29 ms, transmitter offset = 175 ppm, 7-Hz line-broadening.

can have two explanations: (1) production of lactate in the brain tissue, (2) production of lactate throughout the body and transport of lactate into the brain. In normal rat brain, the reported lactate concentration was about 1 mM [52]. Under certain anesthetics such as isoflurane, which was used in this study, higher lactate levels have been observed in the rat brain [52].

Similarly, the bicarbonate signal appears to arise primarily from brain tissue, with little bicarbonate in the subcutaneous tissue voxel. The three-compartment metabolic model indicates that most of the bicarbonate is produced in the brain although a few percent of the signal detected in the brain could be coming from bicarbonate produced in the body and transported to the brain.

In the present study, a T_1 of 14 s was assumed for pyruvate, lactate and bicarbonate *in vivo*. This assumption is based on an estimation of the T_1 of pyruvate in the blood from our own data, as well as on values of T_1 previously reported for pyruvate *in vivo* by other groups. However, precise data for T_1 of ^{13}C compounds is difficult to obtain *in vivo*. It is conceivable, for example, that the T_1 of bicarbonate is longer than the T_1 of pyruvate and lactate *in vivo*. We verified that choosing a longer T_1 for bicarbonate does not significantly alter the results. Nonetheless, since the exact values of fitted metabolic fluxes for PDH and LDH are sensitive to the assumed values of T_1, it will be important to validate and refine these assumptions in future studies.

The appearance of a bicarbonate signal following the injection of [1-^{13}C]pyruvate has been shown in the heart tissue to be exclusively related to PDH flux (V_{PDH}) [35]. Previously, the V_{PDH} in the brain has been obtained using conventional ^{13}C MRS experiments in which ^{13}C-labeling of glutamate was measured during the infusion of ^{13}C-labeled glucose, requiring at least 1 h of infusion. The V_{LDH}, on the other hand, has not been measured using dynamic ^{13}C MRS. Here, we proposed a metabolic model to fit experimental data and determine the values of $V_{PDH\ brain}$ and $V_{LDH\ brain}$. We were able to measure $V_{PDH\ brain}$ within less than 1 min kinetics.

The detection of hyperpolarized lactate and bicarbonate signal in the brain shows that the hyperpolarized state has persisted through multiple steps in pyruvate transport and metabolism. The ability to measure the reaction rates of LDH and PDH enzymes opens new ways to study brain energy metabolism. Adequate regulation of brain energy metabolism is critical for its function. The ability to measure the rates of PDH and LDH in a short time frame (∼1 min) opens up new possibilities for the study of the role of these enzymes under physiological conditions, during functional activation, and in disease.

5. Conclusion

This study demonstrates the first detection of hyperpolarized signals in the brain *in vivo* using both [1-^{13}C]pyruvate and [2-^{13}C]pyruvate and the quantitative metabolic modeling of hyperpolarized data. A metabolic model was used to fit the hyperpolarized ^{13}C time courses obtained during infusion of [1-^{13}C]pyruvate and to determine the values of V_{PDH} and V_{LDH}. The ability to determine values for these metabolic rates with approximately 1 min of data acquisition opens up new avenues for the study of brain metabolism.

Acknowledgments

The authors thank Manda Vollmers, Dee Koski, and William Mander from Oxford Instruments Molecular Biotools for technical support, Michael G. Garwood for helpful discussion about adiabatic pulses, and Josef Granwehr and Jamie D. Walls for comments about the paper. This work was supported by BTRR – P41 RR008079, P30 NS057091, RO1-NS38672, and the W.M. Keck Foundation. The high-resolution NMR facility at the University of Minnesota is supported with funds from the NSF (BIR-961477), the University of Minnesota Medical School, and the Minnesota Medical Foundation.

References

[1] R. Gruetter, In vivo ^{13}C NMR studies of compartmentalized cerebral carbohydrate metabolism, Neurochem. Int. 41 (2002) 143–154.
[2] G. Frossati, Polarization of ^{3}He, D_2 and (eventually) ^{129}Xe using low temperatures and high magnetic fields, J. Low Temp. Phys. 111 (1998) 521–532.

[3] M.A. Bouchiat, T.R. Carver, C.M. Varnum, Nuclear polarization in ^{3}He gas induced by optical pumping and dipolar exchange, Phys. Rev. Lett. 5 (1960) 373–375.
[4] B.C. Grover, Noble-gas NMR detection through noble-gas–rubidium hyperfine contact interaction, Phys. Rev. Lett. 40 (1978) 391–392.
[5] C.R. Bowers, D.P. Weitekamp, Transformation of symmetrization order to nuclear-spin magnetization by chemical reaction and nuclear magnetic resonance, Phys. Rev. Lett. 57 (1986) 2645–2648.
[6] M. Haake, J. Natterer, J. Bargon, Efficient NMR pulse sequences to transfer the parahydrogen-induced polarization to hetero nuclei, J. Am. Chem. Soc. 118 (1996) 8688–8691.
[7] K. Golman, O. Axelsson, H. Johannesson, S. Mansson, C. Olofsson, J.S. Petersson, Parahydrogen-induced polarization in imaging: subsecond ^{13}C angiography, Magn. Reson. Med. 46 (2001) 1–5.
[8] C.R. Bowers, D.P. Weitekamp, Para-hydrogen and synthesis allow dramatically enhanced nuclear alignment, J. Am. Chem. Soc. 109 (1987) 5541–5542.
[9] A. Abragam, M. Goldman, Principles of dynamic nuclear-polarization, Rep. Prog. Phys. 41 (1978) 395–467.
[10] M. Goldman, Spin Temperature and Nuclear Magnetic Resonance in Solids, Oxford University Press, Oxford, 1970.
[11] J.H. Ardenkjaer-Larsen, B. Fridlund, A. Gram, G. Hansson, L. Hansson, M.H. Lerche, R. Servin, M. Thaning, K. Golman, Increase in signal-to-noise ratio of >10,000 times in liquid-state NMR, Proc. Natl. Acad. Sci. U. S. A. 100 (2003) 10158–10163.
[12] J. Wolber, F. Ellner, B. Fridlund, A. Gram, H. Johannesson, G. Hansson, L.H. Hansson, M.H. Lerche, S. Mansson, R. Servin, M. Thaning, K. Golman, J.H. Ardenkjaer-Larsen, Generating highly polarized nuclear spins in solution using dynamic nuclear polarization, Nucl. Instrum. Methods. A 526 (2004) 173–181.
[13] P. Bhattacharya, K. Harris, A.P. Lin, M. Mansson, V.A. Norton, W.H. Perman, D.P. Weitekamp, B.D. Ross, Ultra-fast three dimensional imaging of hyperpolarized ^{13}C in vivo, Magn. Reson. Mater. Phys., Biol. Med. 18 (2005) 245–256.
[14] K. Golman, L.E. Olsson, O. Axelsson, S. Mansson, M. Karlsson, J.S. Petersson, Molecular imaging using hyperpolarized ^{13}C, Br. J. Radiol. 76 SP2 (2003) S118–S127.
[15] E. Johansson, L.E. Olsson, S. Mansson, J.S. Petersson, K. Golman, F. Stahlberg, R. Wirestam, Perfusion assessment with bolus differentiation: a technique applicable to hyperpolarized tracers, Magn. Reson. Med. 52 (2004) 1043–1051.
[16] M. Goldman, H. Johannesson, O. Axelsson, M. Karlsson, Hyperpolarization of ^{13}C through order transfer from parahydrogen: a new contrast agent for MRI, Magn. Reson. Imaging 23 (2005) 153–157.
[17] S. Mansson, E. Johansson, P. Magnusson, C.M. Chai, G. Hansson, J.S. Petersson, F. Stahlberg, K. Golman, ^{13}C imaging – a new diagnostic platform, Eur. Radiol. 16 (2006) 57–67.
[18] L.E. Olsson, C.M. Chai, O. Axelsson, M. Karlsson, K. Golman, J.S. Petersson, MR coronary angiography in pigs with intraarterial injections of a hyperpolarized ^{13}C substance, Magn. Reson. Med. 55 (2006) 731–737.
[19] M. Ishii, K. Emami, S. Kadlecek, J.S. Petersson, K. Golman, V. Vahdat, J.S. Yu, R.V. Cadman, J. MacDuffie-Woodburn, M. Stephen, D.A. Lipson, R.R. Rizi, Hyperpolarized ^{13}C MRI of the pulmonary vasculature and parenchyma, Magn. Reson. Med. 57 (2007) 459–463.
[20] K. Golman, J.H. Ardenkjaer-Larsen, J. Svensson, O. Axelsson, G. Hansson, L. Hansson, H. Johannesson, I. Leunbach, S. Mansson, J.S. Petersson, G. Pettersson, R. Servin, L.G. Wistrand, ^{13}C-angiography, Acad. Radiol. 9 (2002) S507–S510.
[21] K. Golman, J.H. Ardenaer-Larsen, J.S. Petersson, S. Mansson, I. Leunbach, Molecular imaging with endogenous substances, Proc. Natl. Acad. Sci. U. S. A. 100 (2003) 10435–10439.
[22] J. Svensson, S. Mansson, E. Johansson, J.S. Petersson, L.E. Olsson, Hyperpolarized ^{13}C MR angiography using TrueFISP, Magn. Reson. Med. 50 (2003) 256–262.
[23] E. Johansson, S. Mansson, R. Wirestam, J. Svesson, S. Petersson, K. Golman, F. Stahlberg, Cerebral perfusion assessment by bolus tracking using hyperpolarized ^{13}C, Magn. Reson. Med. 51 (2004) 464–472.
[24] K. Golman, J.S. Petersson, Metabolic imaging and other applications of hyperpolarized ^{13}C, Acad. Radiol. 13 (2006) 932–942.
[25] K. Golman, R. in't Zandt, M. Thaning, Real-time metabolic imaging, Proc. Natl. Acad. Sci. U. S. A. 103 (2006) 11270–11275.
[26] K. Golman, R. in't Zandt, M. Lerche, R. Pehrson, J.H. Ardenkjaer-Larsen, Metabolic imaging by hyperpolarized ^{13}C magnetic resonance imaging for *in vivo* tumor diagnosis, Cancer Res. 66 (2006) 10855–10860.
[27] C.H. Cunningham, A.P. Chen, M.J. Albers, J. Kurhanewicz, R.E. Hurd, Y.F. Yen, J.M. Pauly, S.J. Nelson, D.B. Vigneron, Double spin-echo sequence for rapid spectroscopic imaging of hyperpolarized ^{13}C, J. Magn. Reson. 187 (2007) 357–362.
[28] S.J. Kohler, Y. Yen, J. Wolber, A.P. Chen, M.J. Albers, R. Bok, V. Zhang, J. Tropp, S. Nelson, D.B. Vigneron, J. Kurhanewicz, R.E. Hurd, In vivo ^{13}carbon metabolic imaging at 3T with hyperpolarized ^{13}C-1-pyruvate, Magn. Reson. Med. 58 (2007) 65–69.
[29] M.A. Schroeder, L.E. Cochlin, L.C. Heather, K. Clarke, G.K. Radda, D.J. Tyler, R.G. Shulman, *In vivo* assessment of pyruvate dehydrogenase flux in the heart using hyperpolarized carbon-13 magnetic resonance, Proc. Natl. Acad. Sci. U. S. A. 105 (2008) 12051–12056.
[30] D.J. Tyler, M.A. Schroeder, L.E. Cochlin, K. Clarke, G.K. Radda, Application of hyperpolarized magnetic resonance in the study of cardiac metabolism, Appl. Magn. Reson. 34 (2008) 523–531.
[31] A.P. Chen, M.J. Albers, C.H. Cunningham, S.J. Kohler, Y.F. Yen, R.E. Hurd, J. Tropp, R. Bok, J.M. Pauly, S.J. Nelson, J. Kurhanewicz, D.B. Vigneron, Hyperpolarized C-13 spectroscopic imaging of the TRAMP mouse at 3T-initial experience, Magn. Reson. Med. 58 (2007) 1099–1106.
[32] S.E. Day, M.I. Kettunen, F.A. Gallagher, D.E. Hu, M. Lerche, J. Wolber, K. Golman, J.H. Ardenkjaer-Larsen, K.M. Brindle, Detecting tumor response to treatment using hyperpolarized ^{13}C magnetic resonance imaging and spectroscopy, Nat. Med. 13 (2007) 1521.
[33] S. Hu, M. Lustig, A.P. Chen, J. Crane, A. Kerr, D.A.C. Kelley, R. Hurd, J. Kurhanewicz, S.J. Nelson, J.M. Pauly, D.B. Vigneron, Compressed sensing for resolution enhancement of hyperpolarized ^{13}C flyback 3D-MRSI, J. Magn. Reson. 192 (2008) 258–264.
[34] K. Golman, J.S. Petersson, P. Magnusson, E. Johansson, P. Akeson, C.M. Chai, G. Hansson, S. Mansson, Cardiac metabolism measured noninvasively by hyperpolarized ^{13}C MRI, Magn. Reson. Med. 59 (2008) 1005–1013.
[35] M.E. Merritt, C. Harrison, C. Storey, F.M. Jeffrey, A.D. Sherry, C.R. Malloy, Hyperpolarized ^{13}C allows a direct measure of flux through a single enzyme-catalyzed step by NMR, Proc. Natl. Acad. Sci. U. S. A. 104 (2007) 19773–19777.
[36] M.E. Merritt, C. Harrison, C. Storey, A.D. Sherry, C.R. Malloy, Inhibition of carbohydrate oxidation during the first minute of reperfusion after brief ischemia: NMR detection of hyperpolarized $^{13}CO_2$ and H^{13}, Magn. Reson. Med. 60 (2008) 1029–1036.
[37] M.A. Schroeder, H.J. Atherton, D.R. Ball, M.A. Cole, L.C. Heather, J.L. Griffin, K. Clarke, G.K. Radda, D.J. Tyler, Real-time assessment of Krebs cycle metabolism using hyperpolarized 13C magnetic resonance spectroscopy, FASEB J. (2009).
[38] A.P. Chen, J. Kurhanewicz, R. Bok, D. Xua, D. Joun, V. Zhang, S.J. Nelson, R.E. Hurd, D.B. Vigneron, Feasibility of using hyperpolarized [1-^{13}C]lactate as a substrate for in vivo metabolic ^{13}C MRSI studies, Magn. Reson. Imaging 26 (2008) 721–726.
[39] F.A. Gallagher, M.I. Kettunen, S.E. Day, D.E. Hu, J.H. Ardenkjaer-Larsen, R. in't Zandt, P.R. Jensen, M. Karlsson, K. Golman, M.H. Lerche, K.M. Brindle, Magnetic resonance imaging of pH *in vivo* using hyperpolarized ^{13}C-labelled bicarbonate, Nature 453 (2008) 940–973.
[40] P.R. Jensen, R. in't Zandt, M. Karlsson, G. Hansson, S. Mansson, A. Gisselsson, M. Lerche, Acetyl-CoA and acetyl-carnitine show organ specific distribution in mice after injection of DNP hyperpolarized $^{13}C_1$-acetate, Int. Soc. Magn. Reson. Med., Toronto 90 (2008) 892.
[41] F.A. Gallagher, M.I. Kettunen, S.E. Day, M. Lerche, K.M. Brindle, ^{13}C MR spectroscopy measurements of glutaminase activity in human hepatocellular carcinoma cells using hyperpolarized ^{13}C-labeled glutamine, Magn. Reson. Med. 60 (2008) 253–257.
[42] G. Adriany, R. Gruetter, A half-volume coil for efficient proton decoupling in humans at 4 tesla, J. Magn. Reson. 125 (1997) 178–184.
[43] R. Gruetter, Automatic, localized *in vivo* adjustment of all first- and second-order shim coils, Magn. Reson. Med. 29 (1993) 804–811.
[44] R. Gruetter, I. Tkac, Field mapping without reference scan using asymmetric echo-planar techniques, Magn. Reson. Med. 43 (2000) 319–323.
[45] M. Garwood, Y. Ke, Symmetric pulses to induce arbitrary flip angles with compensation for RF inhomogeneity and resonance offsets, J. Magn. Reson. 94 (1991) 511–525.
[46] M. Garwood, L. DelaBarre, The return of the frequency sweep: designing adiabatic pulses for contemporary NMR, J. Magn. Reson. 153 (2001) 155–177.
[47] A.J. Shaka, J. Keeler, T. Frenkiel, R. Freeman, An improved sequence for broad-band decoupling – Waltz-16, J. Magn. Reson. 52 (1983) 335–338.
[48] F. Hyder, A.B. Patel, A. Gjedde, D.L. Rothman, K.L. Behar, R.G. Shulman, Neuronal–glial glucose oxidation and glutamatergic–GABAergic function, J. Cereb. Blood Flow Metab. 26 (2006) 865–877.
[49] S. Xu, J. Yang, J. Shen, In vivo ^{13}C saturation transfer effect of the lactate dehydrogenase reaction, Magn. Reson. Med. 57 (2007) 258–264.
[50] S.V. Gonzalez, N.H. Nguyen, F. Rise, B. Hassel, Brain metabolism of exogenous pyruvate, J. Neurochem. 95 (2005) 284–293.
[51] D.K. Deelchand, A.A. Shestov, D.M. Koski, K. Ugurbil, P.G. Henry, Acetate transport and utilization in the rat brain, J. Neurochem. 109 (Suppl. 1) (2009) 46–54.
[52] J. Pfeuffer, I. Tkac, S.W. Provencher, R. Gruetter, Toward an *in vivo* neurochemical profile: quantification of 18 metabolites in short-echo-time ^{1}H NMR spectra of the rat brain, J. Magn. Reson. 141 (1999) 104–120.
[53] J. Olesen, Total CO_2, lactate, and pyruvate in brain biopsies taken after freezing the tissue in situ, Acta Neurol. Scand. 46 (1970) 141–148.
[54] G. Ahlborg, P. Felig, L. Hagenfeldt, R. Hendler, J. Wahren, Substrate turnover during prolonged exercise in man. Splanchnic and leg metabolism of glucose, free fatty acids, and amino acids, J. Clin. Invest. 53 (1974) 1080–1090.
[55] A.R. Panchal, B. Comte, H. Huang, T. Kerwin, A. Darvish, C. des Rosiers, H. Brunengraber, W.C. Stanley, Partitioning of pyruvate between oxidation and anaplerosis in swine hearts, Am. J. Physiol. Heart Circ. Physiol. 279 (2000) H2390–H2398.
[56] R.L. Veech, R.L. Harris, D. Veloso, E.H. Veech, Freeze-blowing: a new technique for the study of brain in vivo, J. Neurochem. 20 (1973) 183–188.
[57] C.T. Putman, N.L. Jones, E. Hultman, M.G. Hollidge-Horvat, A. Bonen, D.R. McConachie, G.J. Heigenhauser, Effects of short-term submaximal training in humans on muscle metabolism in exercise, Am. J. Physiol. 275 (1998) E132–E139.
[58] B.A. McKinley, W.P. Morris, C.L. Parmley, B.D. Butler, Brain parenchyma PO_2, PCO_2, and pH during and after hypoxic, ischemic brain insult in dogs, Crit. Care Med. 24 (1996) 1858–1868.
[59] J.L. Hall, G.D. Lopaschuk, A. Barr, J. Bringas, R.D. Pizzurro, W.C. Stanley, Increased cardiac fatty acid uptake with dobutamine infusion in swine is accompanied by a decrease in malonyl CoA levels, Cardiovasc. Res. 32 (1996) 879–885.

[60] B.D. Guth, J.A. Wisneski, R.A. Neese, F.C. White, G. Heusch, C.D. Mazer, E.W. Gertz, Myocardial lactate release during ischemia in swine. Relation to regional blood flow, Circulation 81 (1990) 1948–1958.
[61] E.M. Chance, S.H. Seeholzer, K. Kobayashi, J.R. Williamson, Mathematical analysis of isotope labeling in the citric acid cycle with applications to ^{13}C NMR studies in perfused rat hearts, J. Biol. Chem. 258 (1983) 13785–13794.
[62] J.A. Romijn, D.L. Chinkes, J.M. Schwarz, R.R. Wolfe, Lactate–pyruvate interconversion in blood: implications for in vivo tracer studies, Am. J. Physiol. 266 (1994) E334–E340.
[63] R. Gruetter, E.R. Seaquist, K. Ugurbil, A mathematical model of compartmentalized neurotransmitter metabolism in the human brain, Am. J. Physiol. Endocrinol. Metab. 281 (2001) E100–E112.
[64] D.L. Chinkes, X.J. Zhang, J.A. Romijn, Y. Sakurai, R.R. Wolfe, Measurement of pyruvate and lactate kinetics across the hindlimb and gut of anesthetized dogs, Am. J. Physiol. 267 (1994) E174–E182.
[65] S. Broer, H.P. Schneider, A. Broer, B. Rahman, B. Hamprecht, J.W. Deitmer, Characterization of the monocarboxylate transporter 1 expressed in *Xenopus laevis* oocytes by changes in cytosolic pH, Biochem. J. 333 (Pt. 1) (1998) 167–174.
[66] T.J. Barstow, D.M. Cooper, E.M. Sobel, E.M. Landaw, S. Epstein, Influence of increased metabolic rate on [^{13}C]bicarbonate washout kinetics, Am. J. Physiol. 259 (1990) R163–R171.
[67] A.P. Halestrap, A.E. Armston, A re-evaluation of the role of mitochondrial pyruvate transport in the hormonal control of rat liver mitochondrial pyruvate metabolism, Biochem. J. 223 (1984) 677–685.
[68] J.E. Salem, M.E. Cabrera, M.P. Chandler, T.A. McElfresh, H. Huang, J.P. Sterk, W.C. Stanley, Step and ramp induction of myocardial ischemia: comparison of in vivo and in silico results, J. Physiol. Pharmacol. 55 (2004) 519–536.
[69] H.B. Lee, M.D. Blaufox, Blood volume in the rat, J. Nucl. Med. 26 (1985) 72–76.